Nonadiabatic effects on resonance-enhanced two-photon dissociation of H_2

Sima Banerjee, S. S. Bhattacharyya, and Samir Saha
Department of Materials Science, Atomic and Molecular Physics Section, Indian Association for the Cultivation of Science, Jadavpur, Calcutta 700 032, India
(Received 22 June 1993)

Resonance-enhanced two-photon dissociation from the ground $X\,^1\Sigma_g^+$ ($v_g=0,J_g$) state of H_2 to the final continua of *EF*, *GK*, and *I* states has been studied using both linear parallel and crossed polarizations of the two-photon fields. The first field creates an aligned population in the intermediate resonant state $B\,^1\Sigma_u^+$ ($v_i=0,3,J_i$) for which the reduced density-matrix description has been adopted. This intermediate state is dissociated through coherent excitation of a number of near-resonant discrete vibrational levels, bound and quasibound, of $H\bar{H}$ and *I*, respectively, as well as by direct transition to the continua of *EF*, *GK*, and *I* by absorption from the second field. The nonadiabatic interaction of the $H\bar{H}$ and *I* levels with the continuum of *GK* gives these states predissociating characteristics and the whole process can be formulated in terms of overlapping Fano resonances. The nonadiabatic couplings of the continua of *I* and *EF* with the $H\bar{H}$ bound levels have been neglected because of their smallness. The interference of the transition amplitudes to different overlapping predissociating resonances gives the resultant structure in the dissociation probability which is studied for the second photon wavelength covering a range between the dissociation threshold of the final states and the ionization threshold of H_2. The dissociation cross section obtained from these nonadiabatic calculations are found to be drastically altered from the adiabatic and Born-Oppenheimer results.

PACS number(s): 33.80.Gj, 42.50.Hz

I. INTRODUCTION

There has been growing interest in resonance-enhanced multiphoton dissociation and/or ionization (REMPD and/or REMPI) of small diatomic molecules in recent years, both theoretically [1,2] and experimentally [3–6]. In such a process a set of degenerate or near-degenerate levels is coherently excited by resonance absorption and the characteristics of the transition to the continuum then depend upon the symmetry properties and excitation process of this set of coherently excited levels. For sufficiently intense fields, the eigenvalues, eigenfunctions, and symmetry properties of this set may be strongly perturbed by the external electromagnetic fields, and a set of dressed states rather than the field-free set will be effective in determining the transition characteristics. However, in another class of investigations of resonant multiphoton processes weak radiation fields are used and in such cases features such as the transition line shape can be used to explore the intramolecular interactions among states not accessible by single-photon spectroscopy. These interactions, not masked by field effects, play a key role in determining the response of the molecular system to multiphoton excitation. Exact and detailed calculation of the REMPD and/or REMPI cross sections and their comparison with experiment in such cases are useful tools for gaining knowledge of intramolecular interactions. In this context the relevance of resonance-Raman scattering studies (which is basically a two-photon process) for assessing the role of nonadiabatic couplings may also be mentioned [7]. Also it is only for simple diatomic molecules whose electronic potential-energy curves and transition dipole moments are accurately known that such an almost exact and detailed calculation can be meaningfully performed.

In earlier works [1], we studied the resonance-enhanced two-photon dissociation (RETPD) of H_2 in two-frequency weak laser fields assuming the clamped-nuclei or the Born-Oppenheimer (BO) approximation. The calculations were made for parallel, crossed, and circular polarizations of the two-photon fields for different combinations of initial and intermediate rotational levels. However, the nonadiabatic interactions between different electronic states are well known for this smallest two-electron molecule [8,9(a)] [in comparison with other systems [9(b)]]. The knowledge of the nonadiabatic coupling between $B\,^1\Sigma_u^+$ and $C\,^1\Pi_u$ states were used earlier to demonstrate interesting effects on resonance-Raman scattering by H_2 through these states [7]. Another interesting area of investigation is the nonadiabatic couplings between the higher Rydberg state $H\bar{H}\,^1\Sigma_g^+$ and the state $GK\,^1\Sigma_g^+$, and between the $I\,^1\Pi_g$ state and the $GK\,^1\Sigma_g^+$ state [10]. This coupling can be best probed by RETPD. The heterogeneous rotational coupling between *I* and *GK* due to intramolecular configuration interaction mixes the Π^+ and Σ^+ states while the Π^- state remains unperturbed [11]. By restricting the photon intensities to the linear region these intensity-independent effects of intramolecular dynamics on RETPD have been investigated.

More specifically, in this work, we have studied the effect of the above-mentioned nonadiabatic (NA) couplings on RETPD of H_2 for an intermediate resonance with vibrational-rotational levels of the *B* state. The transitions involved are

$$H_2(X\,^1\Sigma_g^+, V_g J_g) \xrightarrow[(\omega_1,\hat{\epsilon}_1)]{\text{vuv}} H_2(B\,^1\Sigma_u^+, v_i J_i)\ ,$$

$$\xrightarrow[(\omega_2,\hat{\epsilon}_2)]{\text{uv or visible}} \left\{ \begin{array}{c} H_2(H\bar{H}\,^1\Sigma_g^+ + I\,^1\Pi_g, v_n J_n) \\ \downarrow NA \\ H_2[(EF+GK)^1\Sigma_g^+ + I\,^1\Pi_g, EJ_f] \end{array} \right\} \rightarrow H(1s)+H(2s/2p)\ .$$

The first photon creates an oriented or aligned population in the intermediate B state. The second photon causes excitation either directly to the dissociation continua of the final EF, GK, and I states or to the vibrational-rotational bound levels of $H\bar{H}$ or quasibound levels of I which act as predissociating levels because of their nonadiabatic couplings with the EF, GK, and I continua. For the weak excitation condition used the nonadiabatic coupling mentioned is rather strong in comparison to the radiative couplings, which indicates the adequacy of the Fano (autoionization) formalism [12,13] for the treatment of this particular excitation step leading to dissociation. However, in this case, a number of predissociating levels of the $H\bar{H}$ and I states could be excited simultaneously and coherently by the second photon. This will cause the amplitudes of the dissociative transitions through these predissociating levels to interfere with each other as well as with the direct transition amplitudes. The Fano asymmetry parameters and the reduced detuning parameters for all the predissociating levels coming together play their part in a complicated form in the line-shape function instead of being simply additive. We have calculated the Fano shape functions along with the dissociation cross sections with all the overlapping resonances. To study the polarization effects, the RETPD cross sections are determined for parallel and crossed polarizations of the two linearly polarized photon fields. We have also computed the adiabatic (AD) cross sections to exhibit the net effect of the nonadiabatic interactions. As in our earlier works [1], the reduced-density-operator method [14] has been used in formulating the first step of the transition.

II. THEORY AND FORMULATION

The RETPD rate at an energy E, considering the interaction of the n overlapping resonances of $H\bar{H}$ bound and I quasibound levels with the final continuum state GK, is given by [1,2(a),12]

$$W_{Eg}^{(2)} = (2\pi/\hbar)[|\langle \Psi_E | H_I | i \rangle|^2 + |\langle E | H_I | i \rangle|^2]\rho_{ii}\ , \tag{1}$$

where H_I is the radiation-molecule interaction Hamiltonian. The first term within the square brackets is due to dissociation to the continuum of GK through predissociating levels of $H\bar{H}$ and I, and the second term corresponds to direct dissociation to the continuum of $I\,^1\Pi_g$. We have, in the steady-state condition for excitation by linearly polarized light [1],

$$\begin{aligned}\rho_{ii} &= \langle i|\rho_i|i\rangle \\ &= (C_1/\Gamma_i)(-1)^{J_g}(2J_i+1)\begin{bmatrix} J_i & 1 & J_g \\ 0 & 0 & 0 \end{bmatrix}^2 \sum_{K_i,M_i} (-1)^{K_i+M_i}(2K_i+1)\begin{bmatrix} 1 & 1 & K_i \\ 0 & 0 & 0 \end{bmatrix} \\ &\times \begin{bmatrix} J_i & J_i & K_i \\ M_i & -M_i & 0 \end{bmatrix}\begin{Bmatrix} 1 & 1 & K_i \\ J_i & J_i & J_g \end{Bmatrix} |\langle R_{0v_iJ_i}(r)|Q_{ig}^{(0)}(r)|R_{0v_gJ_g}(r)\rangle|^2\ ,\end{aligned} \tag{2}$$

where ρ_i is the reduced density operator for the intermediate discrete vibrational-rotational level of $B\,^1\Sigma_u^+$ state (for no J_i or M_i coherence) and

$$C_1 = (4\pi^2/\hbar^2 c) I_1 g(\omega_{ig}-\omega_1)\ . \tag{3}$$

Γ_i is primarily the radiative decay rate due to the spontaneous emission from the intermediate state, I_1 is the intensity, and $g(\omega_{ig}-\omega_1)$ is the normalized line-shape function of the first photon field. $K_i=0,1,2$ determine, respectively, the population (isotropic), orientation, and alignment of the intermediate state, created by the first photon. $Q_{ig}^{(0)}$ is the electronic transition dipole matrix element between the initial and intermediate states.

The radiation interaction Hamiltonian between the intermediate and final states is given by

$$H_I = -(E_2/2)(\hat{\epsilon}_2\cdot\mathbf{d}_2) = -(2\pi I_2/c)^{1/2}(\hat{\epsilon}_2\cdot\mathbf{d}_2)\ , \tag{4}$$

where

$$(\hat{\epsilon}_2\cdot\mathbf{d}_2) = \sum_{p=-1}^{+1}\sum_{\lambda=-1}^{+1} (2)^{-|p|/2}(1-2\delta_{p1})d_\lambda D_{p\lambda}^{1*}(\phi\theta 0)\ , \tag{5}$$

$p=0\,(\pm 1)$ for linear parallel (crossed) polarizations of the two photon fields, I_2 is the intensity, $\hat{\epsilon}_2$ is the unit polarization vector of the second photon field, $\mathbf{d}_2$ is the electric dipole moment operator for transition between the intermediate state $|i\rangle$ and final state $|E\rangle$, and $d_0=d_z$ and $d_{\pm 1}=\mp(2)^{-1/2}(d_x \pm i d_y)$ are the components of $\mathbf{d}_2$ in the body-fixed frame.

The intermediate Σ state wave function $|i\rangle$, the final Σ (Π) continuum state wave function $|E\rangle_\Sigma$ ($|E\rangle_{\Pi^\pm}$), and the predissociating bound Σ state and quasibound Π^+ state wave functions can explicitly be written as

$$|i\rangle=[(2J_i+1)/4\pi]^{1/2}\psi_{i0}(\mathbf{r}_e,r)R_{0v_iJ_i}(r)D^{J_i^*}_{M_i0}(\phi\theta0)\ , \tag{6}$$

$$|E\rangle_\Sigma=(1/4\pi)\sum_{J_f,M_f}(2J_f+1)(i)^{J_f}\exp(-i\delta_{J_f})\psi_{f0}(\mathbf{r}_e,r)R_{0kJ_f}(r)D^{J_f^*}_{M_f0}(\phi\theta0)D^{J_f}_{M_f0}(\phi_k\theta_k0)\ , \tag{7a}$$

$$|E\rangle_{\Pi^\pm}=(1/4\pi)(2)^{-1/2}\sum_{J_f,M_f}(2J_f+1)(i)^{J_f}\exp(-i\delta_{J_f})R_{1kJ_f}(r)$$
$$\times[\psi_{f1}(\mathbf{r}_e,r)D^{J_f^*}_{M_f1}(\phi\theta0)D^{J_f}_{M_f1}(\phi_k\theta_k0)\pm\psi_{f,-1}(\mathbf{r}_e,r)D^{J_f^*}_{M_f,-1}(\phi\theta0)D^{J_f}_{M_f,-1}(\phi_k\theta_k0)]\ , \tag{7b}$$

with

$$rR_{\Lambda kJ}(r)\underset{r\to\infty}{\sim}(2\mu/\pi\hbar^2k)^{1/2}\sin(kr-J\pi/2+\delta_J)\ ,$$

$$|n\rangle_\Sigma=[(2J_n+1)/4\pi]^{1/2}$$
$$\times\psi_{n0}(\mathbf{r}_e,r)R_{0v_nJ_n}(r)D^{J_n^*}_{M_n0}(\phi\theta0)\ , \tag{8a}$$

and

$$|n\rangle_{\Pi}+=[(2J_n+1)/4\pi]^{1/2}(2)^{-1/2}R_{1v_nJ_n}(r)$$
$$\times[\psi_{n1}(\mathbf{r}_e,r)D^{J_n^*}_{M_n1}(\phi\theta0)$$
$$+\psi_{n,-1}(\mathbf{r}_e,r)D^{J_n^*}_{M_n,-1}(\phi\theta0)]\ . \tag{8b}$$

Equation (1) can explicitly be written as [12]

$$W^{(2)}_{Eg}=C_2\left[\left[1+\sum_n q_n/\epsilon_n\right]^2\left\{1+\left[\sum_n 1/\epsilon_n\right]^2\right\}^{-1}\right.$$
$$\left.\times|T^{\Sigma\Sigma}_{Ei}|^2+|T^{\Pi^+\Sigma}_{Ei}|^2+|T^{\Pi^-\Sigma}_{Ei}|^2\right]\rho_{ii}\ , \tag{9}$$

where

$$C_2=(4\pi^2/\hbar c)I_2 \tag{9'}$$

and q_n is the Fano q factor for nonadiabatic coupling of the $H\bar{H}/I$ predissociating state $|n\rangle$ with the continuum of GK. It is defined as

$$q_n=\left[T_{ni}+P\int dE'V_{nE'}T_{E'i}/(E-E')\right]\Big/(\pi V_{nE}T_{Ei})\ . \tag{10}$$

The configuration coupling of the I-state continuum with the $H\bar{H}$ bound levels is negligible [10(a)]. The function

$$f=\left[1+\sum_n q_n/\epsilon_n\right]^2\Big/\left\{1+\left[\sum_n 1/\epsilon_n\right]^2\right\}$$

will be called the Fano shape function [12];

$$\epsilon_n=\{E-E_n-F_n(E)\}/\{\Gamma_n(E)/2\} \tag{11}$$

is the reduced detuning parameter for the nth predissociating level, where E_n is the energy of the nth predissociating level;

$$F_n(E)=P\int(E-E')^{-1}|V_{nE'}|^2dE' \tag{12}$$

represents the shift in the energy E_n due to the interaction of the nth predissociating level with the continuum;

$$\Gamma_n(E)=2\pi|V_{nE}|^2 \tag{13}$$

represents the full linewidth of the predissociating level $|n\rangle$; and

$$V_{nE}=\langle n|V_I|E\rangle \tag{14}$$

is the matrix element of the nonadiabatic coupling Hamiltonian V_I. $\sum_n$ includes all the vibrational-rotational levels of $H\bar{H}$ bound and I quasibound levels embedded within the region between the dissociation threshold of GK, I, and the ionization threshold of H_2. $H\bar{H}$ bound levels only within the inner well of $H\bar{H}$ double-well potential (Fig. 1) [15] are important with respect to coupling. The nonadiabatic interaction of the predissociating levels of $H\bar{H}$ with the continuum of I state is negligible at small internuclear distance (r) [10(a)] and hence it is not considered in our study. The parameters Γ_n, F_n, and q_n are, strictly speaking, functions of E. But in the narrow range of E considered, these may be evaluated with sufficient accuracy at the resonance energy [16(a)].

Using Eqs. (5)–(8), the electric dipole transition matrix elements of the intermediate state with final continuum and predissociating states can be expressed as

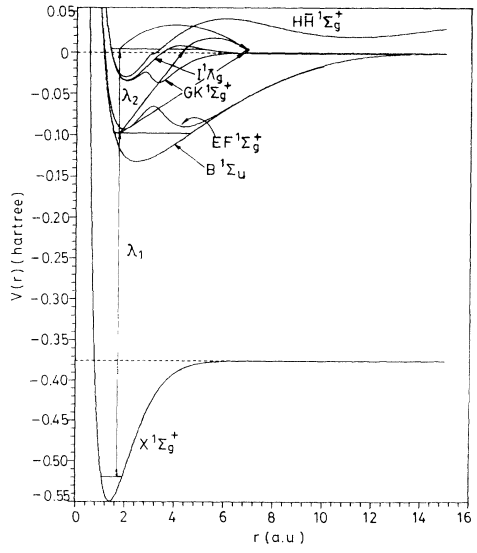

FIG. 1. Plot of the adiabatic potential energies $V(r)$ for the pertinent states of H_2. Excitation from the initial ground state (X) to the intermediate (B) state, then dissociation to the final (EF,GK,I) states either directly or via predissociating levels of $H\bar{H}/I$ states are shown schematically.

$$T_{Ei}^{\Sigma\Sigma}=[(2J_i+1)/4\pi]^{1/2}\sum_{J_f,M_f}(2J_f+1)(i)^{-J_f}\exp(i\delta_{J_f})\sum_p(2)^{-|p|/2}(1-2\delta_{p1})$$
$$\times(-1)^{M_f}\begin{bmatrix}J_f & 1 & J_i\\ -M_f & p & M_i\end{bmatrix}\begin{bmatrix}J_f & 1 & J_i\\ 0 & 0 & 0\end{bmatrix}D^{J_f^*}_{M_f0}(\phi_k\theta_k0)$$
$$\times\langle R_{0kJ_f}(r)|Q_{Ei}^{(0)}(r)|R_{0v_iJ_i}(r)\rangle\ , \tag{15a}$$

$$T_{Ei}^{\Pi^{\pm}\Sigma}=[(2J_i+1)/4\pi]^{1/2}\sum_{J_f,M_f}(2J_f+1)(i)^{-J_f}\exp(i\delta_{J_f})(2)^{-1/2}$$
$$\times\sum_p(2)^{-|p|/2}(1-2\delta_{p1})(-1)^{M_f+1}\begin{bmatrix}J_f & 1 & J_i\\ -M_f & p & M_i\end{bmatrix}\begin{bmatrix}J_f & 1 & J_i\\ 1 & -1 & 0\end{bmatrix}$$
$$\times[(-1)^{J_f+J_i+1}D^{J_f^*}_{M_f1}(\phi_k\theta_k0)\pm D^{J_f^*}_{M_f,-1}(\phi_k\theta_k0)]\langle R_{1kJ_f}(r)|Q_{Ei}^{(1)}(r)|R_{0v_iJ_i}(r)\rangle\ , \tag{15b}$$

$$T_{ni}^{\Sigma\Sigma}=[(2J_n+1)(2J_i+1)]^{1/2}\sum_p(2)^{-|p|/2}(1-2\delta_{p1})(-1)^{M_n}\begin{bmatrix}J_n & 1 & J_i\\ -M_n & p & M_i\end{bmatrix}\begin{bmatrix}J_n & 1 & J_i\\ 0 & 0 & 0\end{bmatrix}\langle R_{0v_nJ_n}(r)|Q_{ni}^{(0)}(r)|R_{0v_iJ_i}(r)\rangle\ , \tag{16a}$$

and

$$T_{ni}^{\Pi^{+}\Sigma}=[(2J_n+1)(2J_i+1)]^{1/2}(2)^{-1/2}\sum_p(2)^{-|p|/2}(1-2\delta_{p1})(-1)^{M_n}\begin{bmatrix}J_n & 1 & J_i\\ -M_n & p & M_i\end{bmatrix}\left\{\begin{bmatrix}J_n & 1 & J_i\\ -1 & 1 & 0\end{bmatrix}+\begin{bmatrix}J_n & 1 & J_i\\ 1 & -1 & 0\end{bmatrix}\right\}$$
$$\times\langle R_{1v_nJ_n}(r)|Q_{ni}^{(1)}(r)|R_{0v_iJ_i}(r)\rangle\ . \tag{16b}$$

The electronic-nuclear rotational matrix elements of the configuration-interaction Hamiltonian are [10]

$$\tilde{V}_{nE}^{\Sigma\Sigma}\left[r,\frac{d}{dr}\right]=A(r)+2B(r)\frac{d}{dr}$$

and

$$\tilde{V}_{nE}^{\Pi_{+1}\Sigma}(r)=(2\mu)^{-1}\{J_n(J_n+1)\}^{1/2}S(r)/r^2\ .$$

The nonadiabatic coupling matrix elements between relevant states are thus

$$V_{nE}^{\Sigma\Sigma}=(4\pi)^{-1/2}\sum_{J_f,M_f}(2J_f+1)^{1/2}(i)^{-J_f}\exp(i\delta_{J_f})D^{J_f^*}_{M_f0}(\phi_k\theta_k0)\left\langle R_{0v_nJ_n}(r)|\tilde{V}_{nE}^{\Sigma\Sigma}\left[r,\frac{d}{dr}\right]|R_{0kJ_f}(r)\right\rangle\delta_{J_fJ_n}\delta_{M_fM_n} \tag{17a}$$

and

$$V_{nE}^{\Pi^{+}\Sigma}=(4\pi)^{-1/2}\sum_{J_f,M_f}(2J_f+1)^{1/2}(i)^{-J_f}\exp(i\delta_{J_f})D^{J_f^*}_{M_f0}(\phi_k\theta_k0)\left\langle R_{1v_nJ_n}(r)|\tilde{V}_{nE}^{\Pi^{+}\Sigma}(r)|R_{0kJ_f}(r)\right\rangle\delta_{J_fJ_n}\delta_{M_fM_n}\ . \tag{17b}$$

It is to be noted that all Γ_n, F_n, ϵ_n, and q_n are to be integrated over all angles [16(b)]. Thus integrating over $\Omega_k(\phi_k\theta_k0)$ we get

$$q_n(\Sigma)=[\langle R_{0v_nJ_n}(r)|Q_{ni}^{(0)}(r)|R_{0v_iJ_i}(r)\rangle+P\int dE'(E-E')^{-1}\langle R_{0v_nJ_n}(r)|\tilde{V}_{nE'}^{\Sigma\Sigma}|R_{0k'J_n}(r)\rangle\langle R_{0k'J_n}(r)|Q_{E'i}^{(0)}(r)|R_{0v_iJ_i}(r)\rangle]$$
$$\times[\pi\langle R_{0v_nJ_n}(r)|\tilde{V}_{nE}^{\Sigma\Sigma}|R_{0kJ_n}(r)\rangle\langle R_{0kJ_n}(r)|Q_{Ei}^{(0)}(r)|R_{0v_iJ_i}(r)\rangle]^{-1}\ . \tag{18}$$

Similarly $q_n(\Pi^+)$ can be obtained by using the Π^+-state wave function and replacing $\tilde{V}_{nE}^{\Sigma\Sigma}(r,d/dr)$ by $\tilde{V}_{nE}^{\Pi^{+}\Sigma}(r)$.

As we are interested in integral dissociation cross sections, we get, after integrating $W_{Eg}^{(2)}$ over $\Omega_k(\phi_k\theta_k0)$,

$$W_{Eg}^{(2)}=\{(16\pi^4I_1I_2)/(\hbar^4c^2\Gamma_i\omega_2)\}g(\omega_{ig}-\omega_1)P_{J_gJ_i}\ , \tag{19}$$

where

$$P_{J_g J_i}=\hbar\omega_2(-1)^{J_g}(2J_i+1)^2\begin{bmatrix}J_i & 1 & J_g\\ 0 & 0 & 0\end{bmatrix}^2|\langle R_{0v_iJ_i}(r)|Q_{ig}^{(0)}(r)|R_{0v_gJ_g}(r)\rangle|^2$$
$$\times\sum_{K_i=0}^{2}(-1)^{K_i}(2K_i+1)\begin{bmatrix}1 & 1 & K_i\\ 0 & 0 & 0\end{bmatrix}\begin{Bmatrix}1 & 1 & K_i\\ J_i & J_i & J_g\end{Bmatrix}\sum_{p=-1}^{+1}(-1)^p(2)^{-|p|}\begin{bmatrix}1 & 1 & K_i\\ p & -p & 0\end{bmatrix}$$
$$\times\sum_{J_f}(-1)^{J_f}(2J_f+1)\begin{Bmatrix}1 & 1 & K_i\\ J_i & J_i & J_f\end{Bmatrix}\Bigg[\begin{bmatrix}J_f & 1 & J_i\\ 0 & 0 & 0\end{bmatrix}^2|\langle R_{0kJ_f}(r)|Q_{Ei}^{(0)}(r)|R_{0v_iJ_i}(r)\rangle|^2$$
$$\times\left[1+\sum_n q_n/\epsilon_n\right]^2\Big/\left\{1+\left[\sum_n 1/\epsilon_n\right]^2\right\}+\begin{bmatrix}J_f & 1 & J_i\\ 1 & -1 & 0\end{bmatrix}^2$$
$$\times|\langle R_{1kJ_f}(r)|Q_{Ei}^{(1)}(r)|R_{0v_iJ_i}(r)\rangle|^2\Bigg]. \tag{20}$$

The generalized integral dissociation cross section is

$$\sigma_{Eg}^{(2)}=W_{Eg}^{(2)}/F_1F_2$$
$$=\{[2^5\pi^5 g(\omega_{ig}-\omega_1)]/(\hbar^2c\lambda_1\Gamma_i)\}P_{J_gJ_i}, \tag{21}$$

where F_1 and F_2 are the photon flux of two laser fields and λ_1 is the wavelength of the first photon field.

III. CALCULATIONS

We have calculated the RETPD cross sections of H_2 molecule for transitions from the initial ground $X\,^1\Sigma_g^+$ ($v_g=0, J_g=0-2$) to the final $[(EF+GK)\,^1\Sigma_g^+ + I\,^1\Pi_g](E,J_f)$ states via the intermediate $B\,^1\Sigma_u^+$ ($v_i=0,3; J_i=0-3$) state for linear polarizations of the two photon fields. The final GK-state continuum is strongly coupled with the predissociating bound levels of the high Rydberg state $H\bar{H}$ and quasibound levels of the state I by nonadiabatic interaction. The Born-Oppenheimer potential energies and the adiabatic corrections to them for the X, B, EF, GK, $H\bar{H}$, and I states are taken from Wolniewicz and Dressler [17,15,10(b)] and others [18]. The radial bound and free wave functions for single-well potential are generated by numerically solving the corresponding radial Schrödinger equations using the Numerov-Cooley method [19(a)]. The bound-state eigenenergies and eigenfunctions for the double-well potential ($H\bar{H}$) are obtained using the Numerov-Cooley method modified by Wolniewicz and co-workers [19(b)]. The I-state quasibound vibrational wave functions are computed following Le Roy and Liu [20] by matching the wave function at the outermost turning point with the Airy functions [21]. The nonadiabatic coupling matrix elements for $H\bar{H}\,^1\Sigma_g^+ - GK\,^1\Sigma_g^+$ vibrational and $I\,^1\Pi_g - GK\,^1\Sigma_g^+$ rotational couplings are given by Quadrelli, Dressler, and Wolniewicz [10(a)] and Dressler and Wolniewicz [10(b)], respectively. The principal-value parts in F_n and q_n are calculated by Gaussian quadrature. The electronic dipole transition moments $d_\lambda(r)$ for X-B and B-GK transitions are obtained from Wolniewicz [22] and Wolniewicz and Dressler [23], and those for B-I are taken from Dressler and Wolniewicz [10(b)]. All the potential energies, transition dipole moments, and coupling matrix elements are interpolated by the cubic-spline-interpolation method [24]. The values of Γ_i and $g(\omega_{ig}-\omega_1)$ are taken from Stephens and Dalgarno [25] and Meier, Zacharias, and Welge [3(b)], respectively.

IV. RESULTS AND DISCUSSIONS

Eigenenergies (E_n), full linewidths (Γ_n), line shifts (F_n), and Fano asymmetry parameters (q_n) for the predissociating bound vibrational-rotational levels of the $H\bar{H}\,^1\Sigma_g^+$ state [levels within the inner well of the double-well potential curve (Fig. 1)] and the $I\,^1\Pi_g$ state (quasi-bound levels) are presented in Table I. For the $H\bar{H}$ state, the vibrational levels 8 and 9 are very close and change of localization occurs at lower J values so that for $v_{H\bar{H}}=8$, all the rotational levels, except $J_{H\bar{H}}=0$, are within the outer well whereas for $v_{H\bar{H}}=9$, $J_{H\bar{H}}=1-4$ are within the inner well. We have not considered contribution from levels with wave functions localized in the outer well of $H\bar{H}$ due to negligible nonadiabatic coupling [10(a)] and very small Franck-Condon overlaps [15].

The Fano shape functions f are plotted against λ_2, the second photon wavelength, in the range between the dissociation threshold of $EF\,^1\Sigma_g^+$, $GK\,^1\Sigma_g^+$, $I\,^1\Pi_g$, and the ionization threshold of H_2. The nonadiabatic coupling of the EF continuum with the predissociating bound levels of $H\bar{H}$ is very weak [10(a)] and the direct dissociation through this state is very small compared to the other two continua of GK and I [1]. Hence the final state EF has not been considered in the present study. The range of λ_2 contains overlapping resonances with the bound $H\bar{H}$ ($v_{H\bar{H}}=3-5,8,9$) and quasibound I ($v_I=4$) levels with selected rotational quantum numbers ($J_{H\bar{H}}$ and J_I) according to the values of J_i (rotational level of $B\,^1\Sigma_u^+$ state), which is fixed in turn by J_g (rotational level of initial $X\,^1\Sigma_g^+$ state); levels with $v_{H\bar{H}}=6$ and 7 are localized into the outer well. Figures 2 and 3 present f values for overlapping resonances with $v_i=0$ and 3, respectively, as functions of λ_2.

Figure 2(a) is for $J_i=1$. Thus the allowed J values are

$J_{H\bar{H}}=0,2$ and $J_I=2$ only (as $J_g=0$). Again the wave function for the $v_{H\bar{H}}=8, J_{H\bar{H}}=2$ level and the $v_{H\bar{H}}=9, J_{H\bar{H}}=0$ level are in the outer well and hence they have not been considered. The individual contribution of each of these levels to f are recognizable in the respective regions of λ_2. In four such regions, the three regions at the right contain resonances with $v_{H\bar{H}}=3$ (overlapped with $v_I=4$), 4, and 5 respectively, whereas the leftmost region is for λ_2 values for resonance with $v_{H\bar{H}}=8,9$. In each region two individual curves corresponding to two final rotational quantum numbers are shown by dashed and dotted curves. However, the two branches due to $J_{H\bar{H}}=0,2$ interfere in their overlapping regions so that the total shape function has interesting structures instead of being the mere sum of the individual contributions. There are destructive minima, one in each region of λ_2. Ranges of λ_2 for resonances with different vibrational quantum numbers are generally well separated and the overlap is negligible. Contributions for $v_{H\bar{H}}=3,8,9$ are of comparably larger value than for $v_{H\bar{H}}=4,5$. However there is strong overlap between the level $v_I=4, J_I=2$ and $v_{H\bar{H}}=3, J_{H\bar{H}}=2$ and they are very closely spaced. This is also true for $v_{H\bar{H}}=8$ and 9. The levels $v_{H\bar{H}}=8, J_{H\bar{H}}=0$ and $v_{H\bar{H}}=9, J_{H\bar{H}}=2$ are very close to each other and the individual shape functions for these vibrational levels appear as two rotational branches of a single vibrational level and interfere, giving a very deep minimum like other regions corresponding to single $v_{H\bar{H}}$. It is interesting to note that contribution from $v_I=4, J_I=2$ is so small that the shape function for this level considered alone does not appear in the figure. But when it is included, the resultant f, $(1+\sum_n q_n/\epsilon_n)^2/\{1+(\sum_n 1/\epsilon_n)^2\}$, changes considerably with a significant destructive dip. Moreover, there is another small modulation in the resultant f due to larger transition probability to the I-state quasibound level, i.e., the shape resonance.

Figure 2(b) is for $J_i=2$, with $J_{H\bar{H}}$ and J_I taking values 1 and 3. In this case for $v_{H\bar{H}}=4$, the two rotational branches interfere constructively throughout the corresponding range of λ_2, whereas for all other $v_{H\bar{H}}$, the overlapping branches show minima. At longer wavelengths, the two rotational branches for $v_{H\bar{H}}=3$ and those for $v_I=4$ overlap and produce a very complex structure in the resultant shape function. For this set also the shape-

TABLE I. Eigenenergies (E_n), full linewidths (Γ_n), line shifts (F_n), and Fano asymmetry parameters (q_n) for predissociating levels of $H\bar{H}$ and I states. $1.04[-3]=1.04\times10^{-3}$.

						q_n			
						$v_i=0$		$v_i=3$	
PS[a]	v_n	J_n	E_n (a.u.)	Γ_n (a.u.)	F_n (a.u.)	$J_i=J_n-1$	$J_i=J_n+1$	$J_i=J_n-1$	$J_i=J_n+1$
$H\bar{H}$	3	0	−0.065 79	1.04[−3]	8.44[−5]		30.74		−9.13
		1	−0.065 59	1.04[−3]	8.82[−5]	29.44	31.08	−9.47	−8.92
		2	−0.065 18	1.05[−3]	9.43[−5]	28.57	31.21	−9.59	−8.69
		3	−0.064 58	1.07[−3]	1.64[−4]	27.78	31.30	−9.56	−8.35
		4	−0.063 78	1.08[−3]	1.03[−4]	26.50		−9.73	
	4	0	−0.059 06	9.14[−4]	−6.32[−5]		12.72		1.73
		1	−0.058 86	9.13[−4]	−6.04[−5]	11.10	12.04	1.62	1.75
		2	−0.058 46	9.10[−4]	−5.51[−5]	7.07	10.50	1.51	1.76
		3	−0.057 87	9.09[−4]	−4.31[−5]	−6.52	7.89	1.38	1.74
		4	−0.057 07	9.10[−4]	−3.21[−5]	516.77		1.24	
	5	0	−0.051 97	1.07[−3]	−1.05[−5]		13.93		−0.06
		1	−0.051 79	1.07[−3]	−9.07[−6]	13.98	13.75	−0.05	−0.07
		2	−0.051 42	1.06[−3]	−7.39[−6]	13.81	13.44	−0.06	−0.09
		3	−0.050 88	1.05[−3]	−5.17[−6]	13.53	13.02	−0.07	−0.12
		4	−0.050 17	1.03[−3]	4.72[−5]	13.63		−0.13	
	8	0	−0.045 80	8.82[−4]	−4.73[−5]		31.16		−0.43
	9	1	−0.045 63	8.84[−4]	−4.65[−5]	29.56	30.55	−0.42	−0.43
		2	−0.045 28	8.87[−4]	−4.48[−5]	27.68	29.01	−0.40	−0.42
		3	−0.044 76	8.93[−4]	−4.22[−5]	25.58	26.87	−0.38	−0.40
		4	−0.044 08	9.02[−4]	−3.87[−5]	23.33		−0.35	
I	4	1	0.004 773	5.17[−5]	1.20[−5]	−0.66	−1.17	13.25	15.87
		2	0.005 133	1.51[−4]	3.53[−5]	−0.55	−1.43	7.56	12.84
		3	0.005 665	2.91[−4]	7.32[−5]	−0.43	1.89	5.41	17.62
		4	0.006 358	4.58[−4]	1.19[−4]	−0.38		5.63	

[a]Predissociating state. E_n are measured from dissociation threshold of the corresponding state.

function curve is much more prominent in the region around the resonance with $v_{H\bar{H}}=3$ ($v_I=4$) and 9 compared to those with $v_{H\bar{H}}=4$ and 5.

Figure 2(c) is a result of $J_i=3$, requiring $J_{H\bar{H}}$ and J_I to be 2 and 4; $v_{H\bar{H}}$ and v_I are same as the preceding case. Unlike the previous two cases, here one q_n value (for $v_{H\bar{H}}=4$, $J_{H\bar{H}}=4$) is larger than those for the other vibrational-rotational branches by an order of magnitude (Table I). The total and individual shape functions have large magnitudes only in the region about the resonance with this level. However, there is interesting structure throughout the whole range of λ_2, and to show this whole structure the curve for resultant shape function is plotted

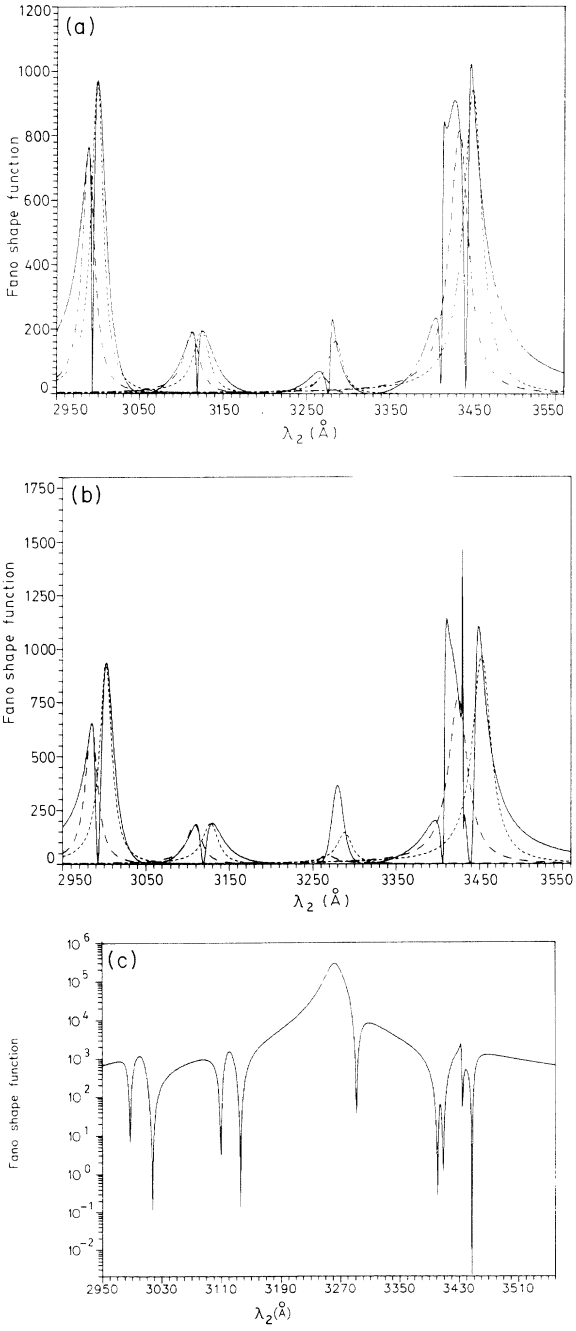

FIG. 2. (a) Fano shape functions against λ_2 with $J_g=0$, $v_i=0$, and $J_i=1$. —— represents the resultant shape function for all v_n and J_n, · · · · represents the individual shape function for $J_n=J_i-1$, and — — — represents the individual shape function for $J_n=J_i+1$. (b) Same as (a) except $J_g=1$ and $J_i=2$. (c) Same as (a) except $J_g=2$ and $J_i=3$. Only the resultant shape function is shown.

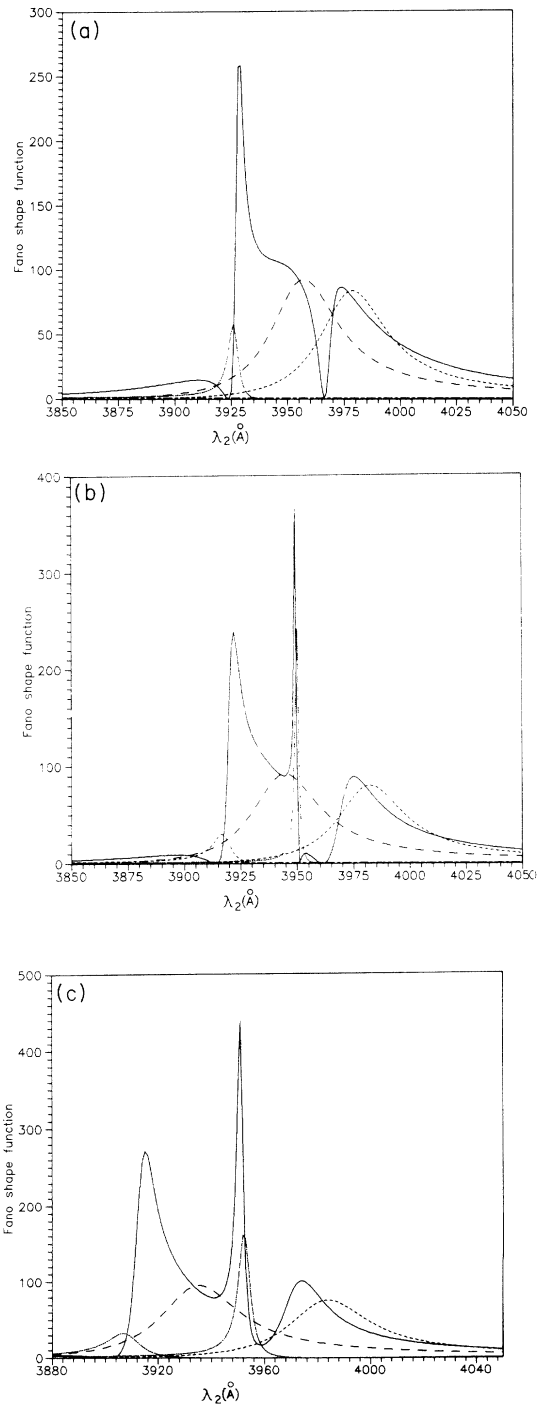

FIG. 3. (a) Same as Fig. 2(a) except $v_i=3$. (b) Same as Fig. 2(b) except $v_i=3$. (c) Same as Fig. 2(c) except $v_i=3$. The resultant and individual shape functions are shown.

in logarithmic scale. To avoid clumsiness, the individual curves have not been plotted. As in the previous case, the higher λ_2 range is more complicated due to presence of both I-state quasibound levels and $H\bar{H}$ bound levels very close to one another.

For $v_i=3$, the nonadiabatic effect is dominant by orders of magnitude at higher wavelengths corresponding to the region about resonance with $v_{H\bar{H}}=3$ and $v_I=4$. Hence the shape functions are plotted only in this region of λ_2. Unlike the $v_i=0$ cases, here the individual shape functions for the I quasibound levels are considerably large.

Figure 3(a) corresponds to $J_i=1$. Individual shape functions for $v_I=4, J_I=2$ and $v_{H\bar{H}}=3, J_{H\bar{H}}=2,0$ appear

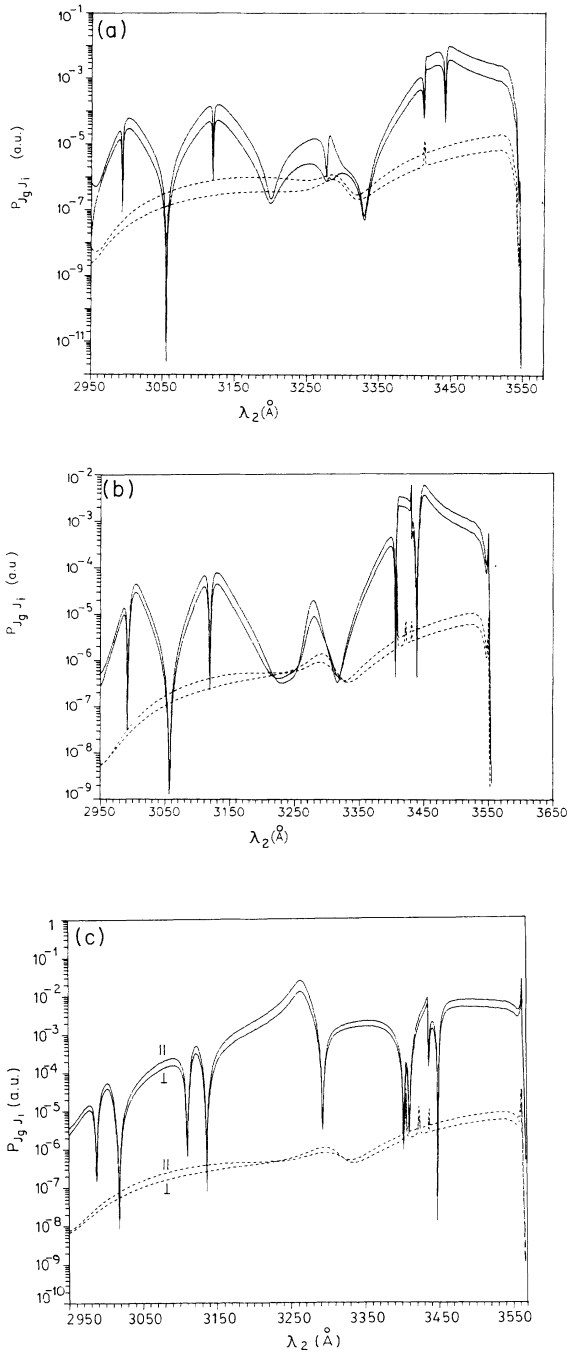

FIG. 4. (a) RETPD cross sections (weighted by some factor) $P_{J_g J_i}$ for $X\,^1\Sigma_g^+$ $(v_g=0, J_g=0) \rightarrow B\,^1\Sigma_u^+$ $(v_i=0, J_i=1)$ $\rightarrow[(EF+GK)\,^1\Sigma_g^+ + I\,^1\Pi_g](E)$ transition for nonadiabatic (——) and adiabatic (· · · ·) cases. (b) Same as (a) except $J_g=1$ and $J_i=2$. (c) Same as (a) except $J_g=2$ and $J_i=3$.

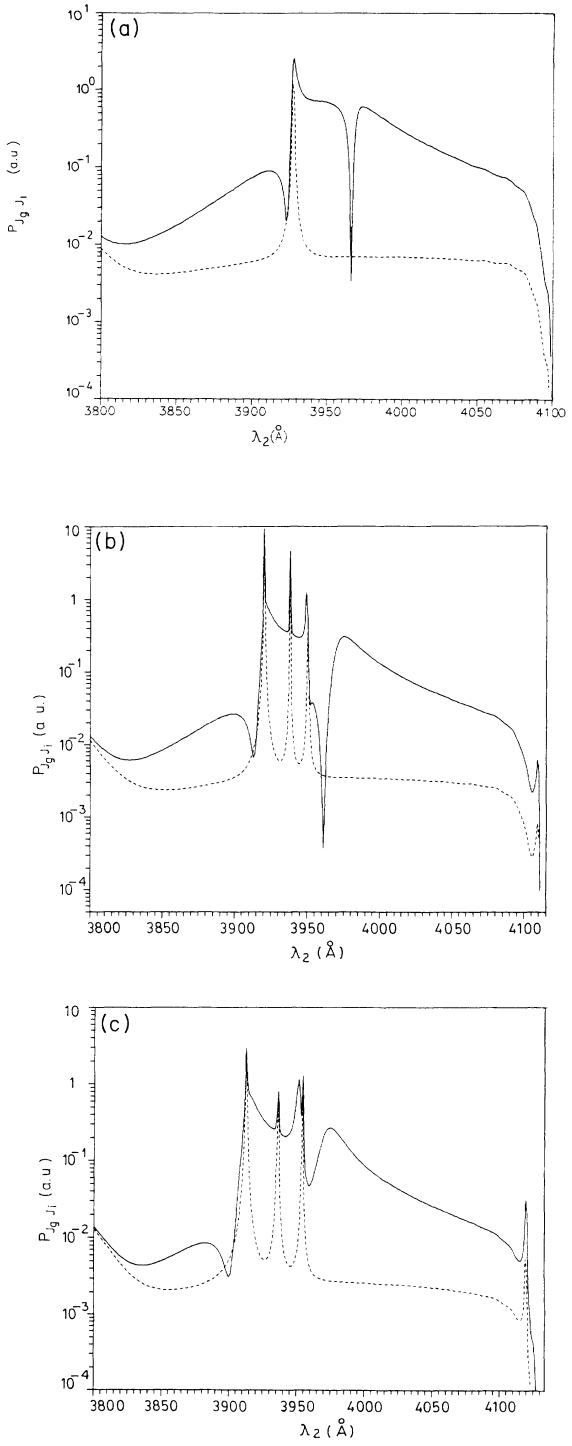

FIG. 5. (a) Same as Fig. 4(a) except $v_i=3$. (b) Same as Fig. 4(b) except $v_i=3$. (c) Same as Fig. 4(c) except $v_i=3$.

TABLE II. Generalized RETPD cross sections $\sigma_{Eg}^{(2)}$ for $X(v_g=0,J_g=0-2)\rightarrow B(v_i=0,3,$ $J_i=0-3)\rightarrow(EF+GK+I)$ transitions with linear (a) parallel and (b) crossed polarizations of the two photon fields, using different methods. $5.353[-10]=5.353\times10^{-10}$.

			$v_i=0$ ($\Gamma_i^{-1}=5.353[-10]$ s)			$v_i=3$ ($\Gamma_i^{-1}=6.510[-10]$ s)		
J_g	J_i	Method	λ_1 (Å)	λ_2 (Å)	$\sigma_{Eg}^{(2)}$ (cm^4 s)	λ_1 (Å)	λ_2 (Å)	$\sigma_{Eg}^{(2)}$ (cm^4 s)
					(a)			
0	1	NA	1108.67	3050	4.35[−46]	1063.36	3550	6.90[−43]
		AD	1108.67	3050	3.23[−46]	1063.36	3550	7.40[−43]
		BO	1108.19	3050	3.83[−46]	1062.83	3550	2.95[−43]
		NA	1108.67	3250	1.42[−44]	1063.36	3750	6.45[−41]
		AD	1108.67	3250	8.86[−46]	1063.36	3750	6.58[−41]
		BO	1108.19	3250	9.84[−46]	1062.83	3750	5.47[−41]
		NA	1108.67	3525	2.19[−42]	1063.36	4050	1.35[−40]
		AD	1108.67	3525	2.01[−44]	1063.36	4050	8.41[−42]
		BO	1108.19	3525	2.40[−44]	1062.83	4050	9.85[−42]
1	2	NA	1109.17	3050	5.03[−46]	1063.93	3550	6.69[−43]
		AD	1109.17	3050	1.79[−46]	1063.93	3550	6.95[−43]
		BO	1108.68	3050	2.11[−46]	1063.40	3550	3.14[−43]
		NA	1109.17	3300	2.07[−45]	1063.93	3800	1.73[−41]
		AD	1109.17	3300	8.75[−46]	1063.93	3800	1.50[−41]
		BO	1108.68	3300	1.17[−45]	1063.40	3800	3.55[−41]
		NA	1109.17	3525	1.06[−42]	1063.93	4050	5.53[−41]
		AD	1109.17	3525	1.12[−44]	1063.93	4050	4.00[−42]
		BO	1108.68	3525	1.20[−44]	1063.40	4050	4.74[−42]
2	3	NA	1110.65	3050	8.53[−44]	1065.46	3550	8.55[−43]
		AD	1110.65	3050	1.62[−46]	1065.46	3550	8.80[−43]
		BO	1110.16	3050	1.90[−46]	1064.92	3550	4.68[−43]
		NA	1110.65	3300	6.95[−43]	1065.46	3800	1.83[−41]
		AD	1110.65	3300	8.11[−46]	1065.46	3800	1.74[−41]
		BO	1110.16	3300	9.41[−46]	1064.92	3800	3.34[−41]
		NA	1110.65	3525	7.52[−42]	1065.46	4050	3.48[−41]
		AD	1110.65	3525	9.10[−45]	1065.46	4050	3.08[−42]
		BO	1110.16	3525	9.60[−45]	1064.92	4050	3.69[−42]
					(b)			
0	1	NA	1108.67	3050	1.71[−46]	1063.36	3550	5.17[−43]
		AD	1108.67	3050	1.27[−46]	1063.36	3550	5.20[−43]
		BO	1108.19	3050	1.50[−46]	1062.83	3550	1.51[−43]
		NA	1108.67	3250	2.76[−45]	1063.36	3750	4.81[−41]
		AD	1108.67	3250	4.64[−46]	1063.36	3750	4.87[−41]
		BO	1108.19	3250	1.56[−46]	1062.83	3750	4.06[−41]
		NA	1108.67	3525	7.09[−43]	1063.36	4050	4.01[−41]
		AD	1108.67	3525	6.50[−45]	1063.36	4050	2.49[−42]
		BO	1108.19	3525	7.90[−45]	1062.83	4050	3.08[−42]
1	2	NA	1109.17	3050	3.10[−46]	1063.93	3550	6.50[−43]
		AD	1109.17	3050	1.11[−46]	1063.93	3550	6.60[−43]
		BO	1108.68	3050	1.31[−46]	1063.40	3550	2.19[−43]
		NA	1109.17	3300	2.15[−45]	1063.93	3800	2.09[−41]
		AD	1109.17	3300	1.32[−45]	1063.93	3800	1.95[−41]
		BO	1108.68	3300	1.77[−45]	1063.40	3800	5.09[−41]
		NA	1109.17	3525	6.09[−43]	1063.93	4050	2.97[−41]
		AD	1109.17	3525	6.46[−45]	1063.93	4050	2.15[−42]
		BO	1108.68	3525	6.96[−45]	1063.40	4050	2.62[−42]
2	3	NA	1110.65	3050	5.74[−44]	1065.46	3550	8.08[−43]
		AD	1110.65	3050	1.09[−46]	1065.46	3550	8.22[−43]
		BO	1110.16	3050	1.28[−46]	1064.92	3550	3.53[−43]
		NA	1110.65	3300	5.06[−43]	1065.46	3800	1.98[−41]
		AD	1110.65	3300	1.09[−45]	1065.46	3800	1.90[−41]
		BO	1110.16	3300	1.31[−45]	1064.92	3800	4.26[−41]
		NA	1110.65	3525	4.83[−42]	1065.46	4050	2.11[−41]
		AD	1110.65	3525	5.48[−45]	1065.46	4050	1.87[−42]
		BO	1110.16	3525	6.21[−45]	1064.92	4050	2.28[−42]

from left to right. The range of considerable contribution from the I state is much smaller and the peak is slightly lower than those from the $H\bar{H}$ levels mentioned. The resultant shape function shows that the interference of two rotational branches of $v_{H\bar{H}}=3$ produces one broader maximum while the $J_I=2$ and $J_{H\bar{H}}=2$ branches interfere constructively, giving rise to a much larger and sharper maximum.

Figure 3(b) is due to $J_i=2$. Thus each of $H\bar{H}$ and I states contributes two branches $J_{H\bar{H}}(J_I)=1,3$, which strongly overlap with one another. The $J_{H\bar{H}}=1$ and 3 branches exhibit two equally broad and high peaks. The $J_I=3$ branch contributes the least, but the $J_I=1$ branch has a very sharp resonance peak. The peak is further enhanced, reflecting the same peak in a larger form in the resultant shape function by combining mainly with the $J_{H\bar{H}}=3$ branch contribution. The two $H\bar{H}$ rotational branches combine and give one broader peak. The $J_I=3$ and $J_{H\bar{H}}=3$ branches interfere to give another large peak at lower λ_2.

Figure 3(c) represents shape functions for $J_i=3$ and correspondingly $J_{H\bar{H}}(J_I)=2,4$. The contributions from the $H\bar{H}$ branches are very similar to that for the case with $J_i=2$. The R branch for the I level also behaves similarly to that for $J_i=2$, but the sharpness of the P branch decreases much compared to that for $J_i=2$, whence the minimum arising from interference of the P branch for I level with the $H\bar{H}$ branches gets broadened and merges with the next minimum at higher λ_2 value arising from the $H\bar{H}$ branches.

Figures 4 and 5 show dissociation profiles for adiabatic and nonadiabatic RETPD for linear polarizations of the two photon fields for $v_i=0$ and 3, respectively. Actually we have plotted $P_{J_g J_i}$, which is the RETPD cross section weighted by a factor $[2^5\pi^5 g(\omega_{ig}-\omega_1)]/(\hbar^2 c\lambda_1\Gamma_i)$, which is a constant with respect to λ_2 [1]. The nonadiabatic structures are obtained more or less by superposing the shape function structures on the adiabatic curves.

For $v_i=0$ (Fig. 4), the I-state continuum has a very small contribution to the dissociation cross section, except of course near the shape resonance peaks. The GK-state continuum is the major channel of dissociation throughout almost the whole range of λ_2. Since the nonadiabatic coupling of the resonant states are with the final GK state only, so for $v_i=0$ the dissociation profile is affected by the shape function throughout the whole λ_2 range. For all sets of J_g,J_i, i.e., 0,1 [Fig. 4(a)]; 1,2 [Fig. 4(b)], 2,3 [Fig. 4(c)], it is observed that the nonadiabatic coupling enhances the dissociation by several orders in magnitudes at all wavelengths except for a few very narrow (pointed in maximum cases) "transmission" windows where deep minima arise in the RETPD cross sections.

For $v_i=3$ (Fig. 5), the dissociation profiles are almost unaffected by nonadiabatic coupling effect except in a small range of higher λ_2 values. Hence only the profiles for this range of λ_2 having significant nonadiabatic coupling effects are shown in the figures. In the other portions, the I state is most active and the GK state is more or less inactive as a dissociating continuum channel. As previously discussed (for $v_i=3$), the Fano shape functions have small ups and downs at lower values of λ_2, which, however, does not change the dissociation profile appreciably from the adiabatic case because of the negligible contribution of the GK continuum. Hence the nonadiabatic and adiabatic curves are compared at higher wavelengths only. The configuration interaction causes enhancement everywhere in this range except at some narrow regions where dissociation is below that obtained from the adiabatic approximation. The curves for $J_g=0,J_i=1$ [Fig. 5(a)] have a simpler structure because of a smaller number of rotational branches due to absence of $J_I=0$ and 1 [1]. For $J_g=1,J_i=2$ [Fig. 5(b)] and $J_g=2,J_i=3$ [Fig. 5(c)], the regions where the I-state shape resonance peaks appear show here a complex structure. At the shape resonance positions, the adiabatic values are approximately equal to the nonadiabatic values, because at those positions the GK continuum contributes negligibly so that the nonadiabatic interaction has no role to play. Figure 5 represents dissociation cross sections for parallel polarizations only. The profiles for crossed polarizations are almost similar and for the sake of clarity these are not shown in the figures.

Tables II contain absolute values of a few integral dissociation cross sections for nonadiabatic coupling, adiabatic and Born-Oppenheimer approximations for some specific values of λ_2. Table II(a) corresponds to linear parallel and Table II(b) corresponds to linear perpendicular polarizations of the two photon fields. The AD and BO values do not differ much, but they are much different from the corresponding NA values at most of the cases. It may be noted that the BO results in Ref. [1] are 16 times larger owing to a different definition of intensity in that work. Also the BO results in Ref. [1] were obtained using axial recoil approximation whereas in the present work no such approximation has been made.

V. CONCLUSIONS

For all sets of intermediate levels investigated the nonadiabatic interaction of the final continuum with the bound or quasibound resonant levels has a large enhancing effect at all λ_2 values except at a few pointed regions. The nonadiabatic interactions give these resonant levels a predissociating character. These predissociating levels must be considered to be coherently excited and all the final channels appear in the equation either as direct dissociation background or as coupled continuum multiplied by large shape functions. Resonance contributions from the predissociating levels largely depend on the intermediate levels, e.g., all the $H\bar{H}$ levels contribute by a large amount for $v_i=0$, but this contribution is decreased a lot for $v_i=3$ (except for $v_n=3$). On the other hand, for $v_i=3$, sometimes the contributions of the I-state quasibound levels exceed that of the $H\bar{H}$ state levels, but for $v_i=0$, the I-state quasibound levels are more or less ineffective compared to the $H\bar{H}$ levels. However, the profiles and tables show that almost throughout the whole range of λ_2, the nonadiabatic coupling generally causes an enormous increase in the RETPD cross sections in comparison to AD or BO values, while creating, at the same time, very narrow transmission windows.

[1] S. Banerjee, M. K. Chakrabarti, S. S. Bhattacharyya, and S. Saha, J. Chem. Phys. **95**, 1608 (1991); **96**, 4974 (1992).

[2] (a) S. N. Dixit and V. Mckoy, J. Chem. Phys. **82**, 3546 (1985); (b) D. C. Jacobs and R. N. Zare, *ibid.* **85**, 5457 (1986); K. M. Chen and E. S. Yeung, *ibid.* **72**, 4723 (1980).

[3] (a) K. H. Welge and H. Rottke, in *Multiphoton Processes,* edited by P. Lambropoulos and S. J. Smith (Springer, Berlin, 1984), p. 151; H. Rottke and K. H. Welge, J. Phys. (Paris) Colloq. **46**, C1-127 (1985); W. Meier, H. Rottke, H. Zacharias, and K. H. Welge, J. Chem. Phys. **83**, 4360 (1985); A. H. Kung, T. Trickl, N. A. Gershenfeld, and Y. T. Lee, Chem. Phys. Lett. **144**, 427 (1988); W. Meier, H. Rottke, and H. Zacharias, in *Resonance Ionization Spectroscopy–88,* IOP Conf. Proc. No. 94 (Institute of Physics and Physical Society, London, 1989), Sec. 2, p. 93; (b) W. Meier, H. Zacharias, and K. H. Welge, Chem. Phys. Lett. **63**, 88 (1989).

[4] J. W. J. Verschur and H. B. van Linden van der Heuvell, Chem. Phys. **129**, 1 (1989).

[5] H. Zacharias, R. Schmeiedl, and K. H. Welge, Appl. Phys. **21**, 127 (1980); H. Zacharias, R. Schmeiedl, and K. H. Welge, J. Mol. Struct. **60**, 239 (1980); D. C. Jacobs, R. J. Madix, and R. N. Zare, J. Chem. Phys. **85**, 5469 (1986).

[6] H. Rudolph, D. L. Lynch, S. N. Dixit, and V. Mckoy, J. Chem. Phys. **84**, 6657 (1986).

[7] S. Banerjee, S. S. Bhattacharyya, and S. Saha, J. Raman Spectrosc. **24**, 317 (1993).

[8] L. D. A. Siebbeles, J. M. Schins, and J. Los, Phys. Rev. Lett. **64**, 1514 (1990); L. D. A. Siebbeles, J. M. Schins, W. J. van der Zande, and J. Los, Phys. Rev. A **44**, 343 (1991); M. Glass-Maujean and L. D. A. Siebbeles, *ibid.* **44**, 1577 (1991); L. D. A. Siebbeles, J. M. Schins, J. Los, and M. Glass-Maujean, *ibid.* **44**, 1584 (1991); J. M. Schins, L. D. A. Siebbeles, J. Los, and W. J. van der Zande, *ibid.* **44**, 4162 (1991); J. M. Schins, L. D. A. Siebbeles, J. Los, and W. J. van der Zande, J. Rychlewski, and H. Koch, *ibid.* **44**, 4171 (1991); L. D. A. Siebbeles, J. M. Schins, W. J. van der Zande, J. A. Beswick, and N. Halberstadt, *ibid.* **45**, 4481 (1992).

[9] (a) M. Glass-Maujean, P. Quadrelli, K. Dressler, and L. Wolniewicz, Phys. Rev. A **28**, 2868 (1983); P. Quadrelli, K. Dressler, and L. Wolniewicz, J. Chem. Phys. **93**, 4958 (1990); (b) A. D. Bandrauk and N. Gélinas, *ibid.* **86**, 5257 (1987).

[10] (a) P. Quadrelli, K. Dressler, and L. Wolniewicz, J. Chem. Phys. **92**, 7461 (1990); (b) K. Dressler and L. Wolniewicz, Can. J. Phys. **62**, 1706 (1984).

[11] H. Lefebvre-Brion and R. W. Field, *Perturbations in the Spectra of Diatomic Molecules* (Academic, London, 1986).

[12] U. Fano, Phys. Rev. **124**, 1866 (1961); U. Fano and J. W. Cooper, *ibid.* **137**, A1366 (1965).

[13] F. H. Mies and M. Krauss, J. Chem. Phys. **45**, 4455 (1966); F. H. Mies, Phys. Rev. **175**, 164 (1968).

[14] A. Omont, Prog. Quantum Electron. **5**, 69 (1977); F. K. Lamb and D. ter Haar, Phys. Rep. **2C**, 253 (1971); M. Broyer, G. Gouedard, J. C. Lehmann, and J. Vigué, Adv. Atm. Mol. Phys. **12**, 165 (1976).

[15] L. Wolniewicz and K. Dressler, J. Chem. Phys. **82**, 3292 (1984).

[16] (a) M. S. Child, Spec. Per. Rep.: Mol. Spectrosc. **2**, 466 (1974); (b) S. N. Dixit, Phys. Rev. A **42**, 6932 (1990).

[17] L. Wolniewicz and K. Dressler, J. Chem. Phys. **88**, 3861 (1988); **85**, 2821 (1986).

[18] W. Kolos, K. Szalewicz, and H. Z. Monkhorst, J. Chem. Phys. **84**, 3278 (1986); W. Kolos and L. Wolniewicz, *ibid.* **41**, 3663 (1964); A. L. Ford, A. M. Greenwalt, and J. C. Browne, *ibid.* **67**, 983 (1977).

[19] (a) J. W. Cooley, Math. Comput. **15**, 363 (1961); (b) W. Kolos and L. Wolniewicz, J. Chem. Phys. **50**, 3228 (1969); L. Wolniewicz and T. Orlikowski; J. Comput. Phys. **27**, 169 (1978).

[20] R. J. Le Roy and W. K. Liu, J. Chem. Phys. **69**, 3622 (1978).

[21] H. A. Antosiewicz, in *Handbook of Mathematical Functions,* edited by M. Abramowitz and I. A. Stegun (Dover, New York, 1972), p. 446.

[22] L. Wolniewicz, J. Chem. Phys. **51**, 5002 (1969).

[23] L. Wolniewicz and K. Dressler, J. Mol. Spectrosc. **96**, 195 (1982).

[24] N. E. Greville, in *Mathematical Methods for Digital Computers,* edited by A. Ralston and H. S. Wilf (Wiley, New York, 1967), Vol. 2, p. 156.

[25] T. L. Stephens and A. Dalgarno, J. Quant. Spectrosc. Radiat. Transfer **12**, 569 (1972).